$SrTiO_3$ and $BaTiO_3$ revisited using the projector augmented wave method: Performance of hybrid and semilocal functionals

Roman Wahl, Doris Vogtenhuber, and Georg Kresse
Faculty of Physics, Center for Computational Materials Science, Universität Wien, Sensengasse 8/12, A-1090 Wien, Austria
(Received 30 April 2008; revised manuscript received 29 July 2008; published 24 September 2008)

The structural, electronic, and phonon properties of the cubic and tetragonal phase of $SrTiO_3$ and $BaTiO_3$ are studied from *ab initio*. The calculations are performed in the projector augmented wave density-functional theory framework using the local density approximation, gradient corrected functionals, and hybrid functional as implemented in the Vienna *ab initio* simulation package. Due to the large variation of theoretical predictions for the frequency of the Γ_{15} (TO1) zone-center phonon mode ($94i-64$ cm^{-1}) special attention is accorded to this particular mode and its volume dependence.

DOI: 10.1103/PhysRevB.78.104116 PACS number(s): 71.15.Mb, 71.15.Ap, 77.80.−e, 77.84.−s

I. INTRODUCTION

ABO_3-type perovskite crystals play an important role in numerous technological applications such as energy conservation processes, catalysis, thermoelectric applications, ion conductors, superconductors, and colossal magnetoresistive materials. In the last 20 years, these compounds have been thoroughly theoretically investigated mainly by using *ab initio* methods, in particular density-functional theory methods.[1,2] In most cases, the local density approximation (LDA) has been used for the exchange and correlation (XC) part of the density functional, and to a lesser extent the generalized gradient approximation by (GGA) [mainly PBE, which is the shorthand for the GGA in the parametrization of Perdew, Burke, and Enzerhof[3] (PBE)] and, in very few cases, hybrid functionals have been applied.[4,5]

Both the LDA and PBE approximations are subject to well-known limitations: within the LDA, the atoms tend to "overbind," which leads to too small equilibrium volumes. Although the PBE functional constitutes an improvement over the LDA for most material properties, it tends to "overcorrect" the unit cell volume. Because of the strong volume dependence of the (anti)ferroelectric instabilities, both approaches cannot be expected to give a quantitative description of ABO_3 perovskite properties. For instance, we will show in this work that in $SrTiO_3$, the ferroelectric (FE) instability depends very sensitively on the applied functional *and* the volume. At the theoretical volume, LDA and GGA give qualitatively different results (GGA is unstable against ferroelectric distortions, LDA is stable), and the situation is not improved by evaluating the properties at the experimental volume (GGA is now stable, LDA unstable against ferroelectric distortion). A quantitative description of the FE instability is therefore clearly out of reach, and worse, present theoretical methods even fail to predict concisely whether $SrTiO_3$ is at all unstable against a ferroelectric distortion.

Obviously, the foremost problem is that none of the commonly used density functionals predict an equilibrium volume close to experiment. To resolve this issue, Wu and Cohen (WC) (Ref. 6) suggested attenuating the exchange enhancement factor in the PBE functional. This approach allows obtaining equilibrium volumes that are much closer to experiment than either LDA or PBE. A similar route was followed by Perdew *et al.*[7] They concisely modified the exchange and correlation enhancement factors with the goal of improving the description of solids and surfaces. With the modified functional (PBEsol) excellent agreement with experiment was found for bulk lattice constants for a wide class of materials. These approaches were partly inspired by the work of Armiento and Mattsson,[8] who used a subsystem approach for simultaneously treating solids and surfaces. The final functional also takes on the form of a generalized gradient functional with similar enhancement factors as the PBEsol functional, and yields almost exactly the same lattice constants as the PBEsol functional.[8,9] One can expect that any of these functionals are more suitable for describing the instability of ferroelectric materials, in particular, the dilemma whether to use the experimental or theoretical volume is reduced.

However, a second issue remains unaddressed by these modified GGA functionals. All local and gradient corrected functionals severely underestimate the band gap. Although it is often argued that density-functional theory is in principle not suitable to predict band gaps, the underestimation leads to a significant overestimation of the static screening properties (a profound ground state property), and a one-to-one correspondence between the band gap error and the static screening properties is observed.[10] Since lattice instabilities are strongly linked to the electronic states at the valence band maximum and conduction band minimum, and because dielectric properties are of fundamental importance for ferroelectric materials, an improved description of the band gap and screening properties might be equally important as an improved description of the equilibrium volume.

Hybrid functionals such as B3LYP, PBEh, and HSE06 address this point by partly including the exact nonlocal exchange of Hartree-Fock theory.[11–14] These functionals yield generally much improved band gaps and dielectric properties for extended systems,[14–16] and simultaneously the PBEh and HSE06 functional improve the equilibrium volume.[17] Only the B3LYP functional increases the equilibrium volume, a result of the incorrect behavior of the LYP correlation energy for homogeneous systems, and it is therefore not well suited for the description of extended systems.[18]

In the present work, we decided to focus our investigations on two "classical" model perovskite crystals, strontium

titanate [$SrTiO_3$ (STO)], and barium titanate [$BaTiO_3$ (BTO)]. STO is probably the best investigated ABO_3 perovskite-type oxide due to its extraordinary low-temperature behavior. Above the critical temperature (T_c) of about 105.5 ± 0.5 K (Refs. 19 and 20) it has the usual cubic perovskite structure (O_h).

Decreasing the temperature below T_c, STO undergoes an antiferrodistortive (AFD) structural phase transition to a tetragonal phase lowering the symmetry from O_h to D_{4h} induced by the condensation of a soft phonon mode at the R point.[21] This phase transition involves a rotation of the TiO_6 octahedron around one of the unit cell axes and consequently, due to the decreasing distance between the rotated oxygen and the strontium in the cube corner, an increase in the c lattice constant. This rotation takes place in opposite directions in adjacent unit cells.

In the last ten years renewed interest in the low-temperature phase of $SrTiO_3$ has emerged because of experiments on the static dielectric constant by Müller and Burkard,[23] and Rupprecht and Bell.[24] They showed that the dielectric constant in the cubic phase closely follows the Curie-Weiss law of the form $\epsilon \approx (T - T_{\text{ferro}})^{-1}$ with a critical temperature of 35.5 and 37 K, respectively.

In addition Viana *et al.*[25] showed that, applied to the low temperature tetragonal phase, the Curie-Weiss law yields a critical temperature of about 20 K. However, the predicted transition to the FE phase at T_{ferro}, which is caused by the condensation of a Γ-point phonon forming Ti-O dipoles, was never observed in experiment. Instead of the predicted divergence according to the Curie-Weiss law, the static dielectric constant saturates at an enormous value of approximately 2.4×10^4 when the temperature approaches zero.[23] Therefore $SrTiO_3$ is called an *incipient ferroelectric* material. Additional evidence that $SrTiO_3$ is close to a ferroelectric state is provided by the experiments done by Uwe and Sakudo,[26] which induced the ferroelectric state by applying uniaxial stress, and Itoh *et al.*,[27] who found a transition temperature of 23 K by isotopical substitution of ^{16}O with ^{18}O.

It was first suggested by Müller and Burkard[23] that zero-point quantum fluctuations of the titanium atoms suppress the condensation of the FE-phonon mode, leading to a so called "quantum paraelectric state." This assumption was corroborated later by Jauch and Palmer[28] using γ-ray diffraction and theoretically anticipated by Zhong and Vanderbilt.[29] From experiment, one can thus conclude that, neglecting quantum effects, STO should show a ferroelectric instability at the experimental volume. However, literature gives ambiguous results for the theoretically predicted frequency of the FE-phonon mode ranging from soft to hard ($94i - 64$ cm^{-1}), strongly depending on the chosen volume of the unit cell and the applied functional. We will address this point by carefully evaluating the volume dependence of the phonon frequencies using different functionals. The LDA, PBE, PBEsol, and HSE06 functional will be covered in the present study.

$BaTiO_3$, on the other hand, is a prototypical ferroelectric perovskite, which has the typical perovskite cubic structure at high temperatures. At 393 K it undergoes a structural phase transition to a tetragonal ferroelectric phase. Between 278 and 183 K it has an orthorhombic structure, and below 183 K it has rhombohedral structure.[30] In this paper we will focus our investigations only on the paraelectric cubic and ferroelectric tetragonal phase.

The paper will be organized as follows: The basic computational setups including a brief summary of the applied GGA and hybrid functionals is given in Sec. II. Section III comprises a discussion of the structural properties of the cubic and antiferrodistortive phases of STO and the ferroelectric tetragonal phase of BTO (Sec. III A), comparing our results to experimental, as well as recently published theoretical results. The electronic structures are shortly summarized in Sec. III B, followed by the discussion of the phonon modes of STO and BTO in Sec. III C. In particular, we focus on the variation of the TO phonon modes upon varying cell volumes and exchange-correlation functionals. Finally, our conclusions are given in Sec. IV.

II. COMPUTATIONAL DETAILS

We used the *Vienna ab initio simulation package* (VASP) (Refs. 31 and 32) for the present calculations. The projector augmented wave (PAW) atomic reference configuration was $3s^2 3p^6 3d^2 4s^2$ ($r_s = 0.953$ Å, $r_{p,d} = 1.217$ Å) for Ti, $2s^2 2p^4$ ($r_s = 0.794$ Å, $r_p = 0.979$ Å) for O, $4s^2 4p^6 5s^2$ ($r_{s,p} = 1.323$ Å) for Sr in STO, and $5s^2 5p^6 6s^2$ ($r_s = 1.482$ Å, $r_p = 1.429$ Å) for Ba in BTO, where only electrons treated as valence electrons are explicitly enumerated and the specific core radii are given in brackets for each potential.

Since perovskite properties are strongly dependent on the precise electronic structure, an accurate sampling of the Brillouin zone is of outermost importance. We performed a series of calculations using different Monkhorst-Pack[33] k-point meshes and different cutoff energies for all functionals. It turned out that a $6 \times 6 \times 6$ Monkhorst-Pack k mesh for the Brillouin-zone integration and 500-eV cutoff energy yield sufficiently converged results for the lattice parameters and the bulk moduli of the simple cubic perovskite unit cell. Due to the doubling of the unit cell in the tetragonal phase of STO as described later, a reduced mesh of $4 \times 4 \times 4$ points is sufficiently dense to yield reliable results for this phase. As BTO does not undergo an AFD distortion, a $6 \times 6 \times 6$ k mesh was used for all considered phases. For phonon calculations, a denser mesh is necessary: $8 \times 8 \times 8$ k points are required for the cubic phase of STO and BTO. Due to the required high accuracy of the results, the electronic and ionic convergence criteria had to be chosen much more stringent than for standard bulk calculations. The geometries were relaxed until the maximum remaining force was smaller than 0.005 eV/Å.

As mentioned in the Introduction, the PBEsol functional is a revised form of the standard PBE functional. In the GGA approximation, the XC energy functional is given by

$$E_{xc}^{\text{PBE}}[n(\mathbf{r})] = \int n(\mathbf{r}) \{ e_x^{\text{unif}}[n(\mathbf{r})] F_x(s, \mu) + e_c^{\text{unif}}[n(\mathbf{r})] F_c[n(\mathbf{r}), t, \beta] \} d\mathbf{r}, \quad (1)$$

where e_x^{unif} and e_c^{unif} are the exchange and correlation energy densities per particle for the uniform electron gas, F_x and F_c

TABLE I. Comparison of calculated and experimental lattice constants of STO and BTO in the cubic phase for several GGA and hybrid functionals.

	LDA	PBE	PBEsol	WC	HSE	B3LYP	B3PW	B1-WC	Experiment
					$SrTiO_3$				
a_0 (Å)									
Present	3.863	3.943	3.898		3.904				3.890,[a] 3.900[b]
Ref. 37	3.86	3.93				3.94			
Ref. 38	3.86	3.94				3.94			
Ref. 39	3.878	3.94							
Ref. 4								3.880	
Ref. 5							3.912		
B_0 (GPa)									
Present	198	168	185		192				179[a]
Ref. 37	215	195				187			
Ref. 38	214	169				177			
Ref. 39	191	169							
					$BaTiO_3$				
a_0 (Å)									
Present	3.953	4.035	3.986		3.995				4.00[a]
Ref. 38	3.96	4.03				4.04			
Ref. 4	3.958	4.035		3.990		4.036		3.971	
B_0 (GPa)									
Present	189	162	177		181				162[a]
Ref. 38	196	175				176			
Ref. 40	195	160							

[a]Reference 36.
[b]Reference 20.

are enhancement factors, t and s are density and reduced density gradients, and μ and β are scaling coefficients (for a detailed discussion see Ref. 7.) For PBEsol these scaling coefficients are tuned in such a way that the functional performs better in describing the structural equilibrium properties of solids and their surfaces.

The HSE03 and HSE06 functionals are based on the "parameter-free" PBEh hybrid functional (sometimes also termed PBE0 or PBE1PBE),[12,34] which itself is constructed by mixing 25% nonlocal Fock exchange E_x with 75% PBE exchange[3] E_x^{PBE}:

$$E_{xc}^{\mathrm{PBEh}} = \tfrac{1}{4}E_x + \tfrac{3}{4}E_x^{\mathrm{PBE}} + E_c^{\mathrm{PBE}}. \quad (2)$$

A drawback of this functional is the slow convergence of the exact nonlocal exchange interaction with distance, necessitating dense k-point grids. To overcome this problem, Heyd *et al.*[35] proposed a decomposition of the exact nonlocal exchange into a long- and a short-range part in real space:

$$E_{xc}^{\mathrm{HSE}} = \tfrac{1}{4}E_x^{\mathrm{sr},\mu} + \tfrac{3}{4}E_x^{\mathrm{PBE,sr},\mu} + E_x^{\mathrm{PBE,lr},\mu} + E_c^{\mathrm{PBE}}. \quad (3)$$

The range separation parameter μ controls the characteristic distance at which the long-range nonlocal interaction becomes negligible. Based on a slightly erroneous implementation, Heyd originally proposed a value of $\mu=0.15$ a.u.$^{-1}$ ≈ 0.3 Å^{-1} for the range separation parameter, whereas recently Krukau *et al.*[14] suggested to use $\mu=0.11$ a.u.$^{-1}$ $=0.207$ Å^{-1}. The implementation using the latter range separation parameter is usually termed HSE06, whereas for the first one the abbreviation HSE03 is common. We use a variant of the HSE06 functional that observes the homogeneous electron gas limit and all important sum rules. Contrary to the conventional HSE06 functional, the screening parameter is set to $\mu=0.300$ Å^{-1} in both the semilocal, as well as nonlocal part of the exchange functional, whereas the recommended choice is $\mu=0.207$ Å^{-1}. As has been shown previously, the specific choice of the screening parameter μ has very little influence on the total energies, but slightly affects band gaps.[14,17] From now on we will refer to this functional as HSE. A detailed discussion of the implementation of the real space HSE functional in VASP is given in Ref. 17.

III. RESULTS

A. Structural properties

The equilibrium lattice constants and bulk moduli of STO and BTO in the high-temperature cubic phases were obtained by fitting the volume and corresponding energy data to the Murnaghan equation of state. As one can see in Table I, our standard LDA and PBE results are in good overall agreement with previous calculations. As expected LDA underestimates the lattice constants by approximately 1%, whereas the PBE functional overestimates it by the same amount. The GGA

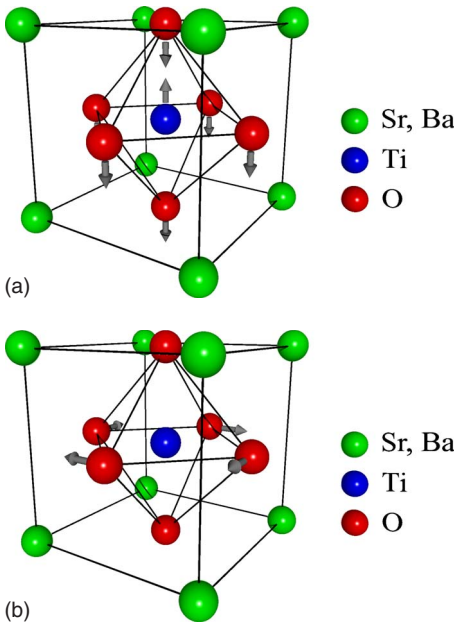

FIG. 1. (Color online) Schematic description of the FE and AFD distortions in STO and BTO, respectively.

functional PBEsol performs significantly better in determining the equilibrium lattice constant for both perovskites. The deviation from the experimentally observed values is only $\approx 0.05\%$. The performance of the hybrid functional HSE is roughly similar, although a trend to slightly larger lattice constants and harder bulk moduli is clearly visible.

The B3LYP hybrid functional predicts lattice constants similar to PBE,[18] whereas the B3PW hybrid functional, which possesses a similar correlation as HSE, also predicts similar lattice constants as HSE. The recently proposed B1-WC hybrid functional[4] combines the gradient-corrected Wu-Cohen functional,[6] which behaves generally very similar to PBEsol, with 16% nonlocal exact exchange. Since the WC exchange functional shrinks the lattice constants compared to PBE, and inclusion of exact exchange reduces the lattice constants even further, this functional predicts lattice constants that are smaller than for PBEsol and HSE.

To be able to describe the AFD structure of $SrTiO_3$ (see Fig. 1), one has to choose a supercell with twice the volume of the cubic unit cell. Due to the clockwise and neighboring anticlockwise rotation of the TiO_6 octahedra around the z axis, the size of the unit cell doubles to $\sqrt{2}\times\sqrt{2}$ in the $x-y$-plane (see inset of Fig. 1 in Ref. 50). Furthermore, in addition to the in-plane rotation of the TiO_6 octahedra, the AFD structure involves a rotation of octahedra against each other in adjacent layers of STO in z direction. In order to use the smallest possible unit cell the z axis has to be tilted such that it points, in the next layer, to a cell with the same sense of rotation for the TiO_6 octahedron. For $BaTiO_3$, the FE phase transition involves a distortion of Ti and O in z direction only (see Fig. 1), and hence a supercell is not required to model the distortion.

In the case of $SrTiO_3$, the relaxation into the AFD equilibrium structure was performed by rotating the oxygen ions out of the cubic equilibrium position, and performing a damped molecular-dynamics simulation in which the lattice shape and size was allowed to change. For the relaxation of BTO into the ferroelectric tetragonal structure, a similar approach was adopted.

Lixin Cao *et al.*[20] measured the temperature dependence of the lattice parameters of bare and epitaxially stressed STO between 65 and 125 K using x-ray backscattering. From the observed temperature dependence of the lattice parameters a and c, as shown in Fig. 4(a) of Cao *et al.*,[20] one can estimate, that at $T=65$ K, c is almost identical to its zero-temperature value (3.9006 Å), whereas some further decrease of a is to be expected (3.8982 Å), thereby increasing c/a as $T=0$ K is approached. In addition to the c/a ratio the rotation angle of the oxygen octahedron is a characteristic criterion to estimate the quality of the used functional.

As expected, one obtains a similar behavior for the equilibrium lattice constants of the AFD phase as for the cubic phase, i.e., LDA and PBE underestimate and overestimate the volume, respectively (see Table II). Furthermore, LDA and PBE both overestimate the rotation angle and the c/a ratio significantly, LDA overestimating more than PBE. PBEsol yields properties in between the two extremes, LDA and GGA. For the volume this is desirable, and in fact the equilibrium volume is very well described by PBEsol. However, the c/a ratio and the rotation angle are much too large as it is the case for LDA and PBE. The hybrid functional HSE performs exceptionally well, much better than any of the gradient-corrected functionals. In particular, the c/a ratio and the rotation angle are very close to experiment, whereas the volume is slightly overestimated compared to the measurements of Heidemann and Wettengel[42] at 10 K. Previous studies utilizing atomic basis sets within the CRYSTAL code (Refs. 5, 37, and 38) give results almost identical to our study for both semilocal (LDA, PBE) and hybrid functionals (B3PW). One can thus conclude that inclusion of Fock exchange weakens the tendency of STO to undergo an antiferrodistortive phase transition, whereas modifications of the density-functional part alone have little influence on the magnitude of the displacement in the antiferrodistortive phase transition.

In the tetragonal phase of BTO, the c/a ratio and the distortions of the titanium and oxygen ions are the relevant properties for the description of the tetragonal ferroelectric phase. Although LDA underestimates, as expected, the lattice parameters and the unit-cell volume, it gives very good results for the c/a ratio and reasonable, but too small results for the displacements of the titanium and oxygen ions. The PBE functional strongly overestimates the c/a ratio and the oxygen and titanium displacements. PBEsol again yields values that are in between LDA and PBE and therefore agreement with experiment is overall very good.

We found that the magnitude of the ferroelectric displacement depends strongly on the volume; it is fairly small for the LDA volume, and almost doubles for the PBE volume. The functional itself has little direct influence on the displacement pattern, e.g., if the c/a ratio and displacement pattern is predicted using the PBE *at the LDA volume*, results are very close to the LDA values.

In Fig. 2 we show the displacement of the Ti atom and the c/a ratio for various volumes evaluated using the PBE func-

TABLE II. Structural properties of the antiferrodistortive phase of $SrTiO_3$ below the critical temperature T_c. θ_z is the rotational angle of the octahedra around the z axis, and $\Delta E = E - E_{AFD}$ describes the energy gain for the antiferrodistortive phase.

	LDA	PBE	PBEsol	HSE	B3PW	Experiment
a (Å)						
Present	3.847	3.933	3.886	3.900		3.898[a] (65 K), 3.898[b] (78 K)
Ref. 5					3.910	
c/a						
Present	1.008	1.004	1.006	1.001		1.0009[c] (10 K), 1.00056[a] (65 K)
Ref. 5					1.0006	
θ_z (°)						
Present	6.05	4.74	5.31	2.63		2.1[d] (4.2 K), 1.4[d] (77 K)
Ref. 5					1.95	
ΔE (eV)						
Present	0.019	0.007	0.011	0.002		
Ref. 5					0.0002	

[a]Reference 20.
[b]Reference 41.
[c]Reference 42.
[d]Reference 43.

tional and using various functionals at their respective equilibrium volumes. Our data calculated using different functionals and the data for B1-WC and B3LYP available from literature[4,38] fit very well on this curve, if we use the volume as control parameter. In this specific case, the predicted volume is therefore the single most important parameter determining the magnitude of the ferroelectric distortion. This behavior agrees well with the fact that BTO is a B-site-driven ABO_3 perovskite, where the titanium ion is too small for its site due to the enlarged cell volume caused by the barium ions at the cube corners (see below).

In this light, it is not astonishing that the GGA functionals PBEsol and WC, as well as the hybrid functional B1-WC, give overall the best description of the distortion because they yield the best volumes, followed by the HSE functional as can be seen in Table III. The macroscopic polarization P can also be seen as a quality criterion for the performance of the different functionals and was calculated using the Berry phase approach.[45,46] The polarization is a result of the ferroelectric distortion. Due to the underestimation of the ionic displacements using the LDA functional the polarization is too small in comparison to the experimentally found value, whereas for PBE the overestimation of the displacement of the titanium and oxygen ions leads to a too large value. As stated above the PBEsol, WC and B1-WC functionals describe the ferroelectric phase best and therefore yield values closest to the experimental data. The HSE hybrid functional overestimates the displacement of the oxygen atoms by a factor of two and yields a too large polarization.

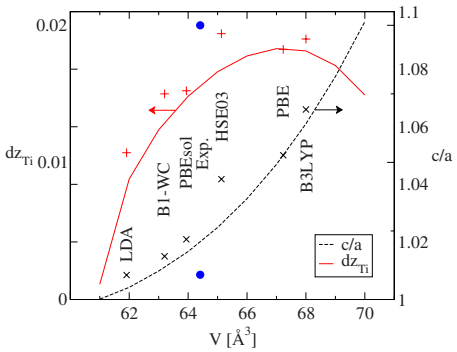

FIG. 2. (Color online) Volume dependence of the c/a ratio (dashed line) and of the relative displacement of Ti ion (dz_{Ti}, solid red line) in the tetragonal phase of $BaTiO_3$ using the PBE functional. Symbols represent results using various functionals at their theoretical equilibrium volume.

B. Electronic properties

For the converged lattice constants of STO and BTO, we have calculated the density of states by using the tetrahedron method for the Brillouin-zone sampling. Table IV shows the direct ($\Gamma-\Gamma$) and indirect ($R-\Gamma$) band gaps for both the cubic and tetragonal distorted structure, and the results from former calculations and experiments.

We observe for both perovskites the well-known behavior for LDA, PBE, and PBEsol: LDA and PBE quite significantly underestimate the band gap, and PBEsol essentially gives results equivalent to LDA and PBE. Due to the fact that the WC functional is a GGA functional it suffers from the same drawbacks concerning electronic properties as all other GGAs.

As expected, the hybrid functionals perform best in comparison to experiment. The B1-WC functional overestimates the band gaps approximately by the same amount as the HSE functional underestimates it. Only in the case of the ferroelectric distorted BTO the B1-WC functional almost exactly reproduces the experimentally observed band gap, whereas the HSE result is 0.4 eV off.

TABLE III. Structural properties and macroscopic polarization P of the ferroelectric tetragonal phase of $BaTiO_3$, where a and c are the fully relaxed lattice parameters, c/a is the tetragonal distortion, V the unit cell volume, and $dz_{O_\perp}$ and $dz_{O_\parallel}$ the atomic displacements parallel to z axes in fractions of the c lattice constant.

	LDA	PBE	PBEsol	WC	HSE	B3LYP	B1-WC	Experiment
a (Å)								
Present	3.945	4.005	3.971		3.969			3.997,[a] 3.986[b]
Ref. 4	3.954	4.013		3.982		3.996	3.962	
c (Å)								
Present	3.978	4.210	4.054		4.135			4.031,[a] 4.026[b]
c/a								
Present	1.009	1.050	1.021		1.042			1.0086,[a] 1.0100[b]
Ref. 4	1.006	1.035		1.012		1.066	1.015	
V (Å^3)								
Present	61.91	67.23	63.94		65.13			64.41,[a] 63.97[b]
Ref. 4	62.2	66.9		63.9		68.0	63.2	
dz								
Present	0.011	0.018	0.015		0.019			0.020,[a] 0.015[b]
Ref. 4	0.011	0.018		0.013		0.019	0.015	
$dz_{O_\parallel}$								
Present	−0.017	−0.047	−0.028		−0.042			−0.026,[a] −0.023 [b]
Ref. 4	−0.014	−0.039		−0.022		−0.057	−0.024	
$dz_{O_\perp}$								
Present	−0.011	−0.027	−0.017		−0.022			−0.012,[a] −0.014 [b]
Ref. 4	−0.009	−0.022		−0.013		−0.031	−0.014	
P (C/m^2)								
Present	0.216	0.435	0.314		0.407			0.27[c]
Ref. 4	0.20	0.39		0.26		0.48	0.28	

[a]Reference 30 measured at 280 K.
[b]Reference 22.
[c]Experimental data from Ref. 44.

C. Phonon properties

With five atoms in the unit cell and 12 degrees of freedom (disregarding the translational mode), the perfect cubic perovskites exhibit four distinct phonon modes: three triply degenerate phonon modes with the irreducible representation Γ_{15}, and one triply degenerate phonon mode with the irreducible representation Γ_{25}. In the present case, we have not calculated the LO-TO splitting, and will therefore restrict our discussion to TO modes.

In Tables V and VI we present our results and the theoretical and experimental data from other publications. Concerning the phonon frequencies, we see from experiment[52,53] that an optical absorption feature is observed for $SrTiO_3$ at room temperature around 90 cm^{-1}, and that this absorption feature drops in frequency when the temperature is lowered. However, this mode [Γ_{15} (TO1)] is certainly not related to a harmonic phonon mode: as already discussed in Sec. I, $SrTiO_3$ shows a divergence of the dielectric constant at low temperature, which indicates that the Γ_{15} (TO1) mode should be soft in a *harmonic* description.

It is immediately obvious that the theoretically predicted phonon frequencies show a huge scatter for $SrTiO_3$, in particular, for the low-frequency soft Γ_{15} mode. Sai and Vanderbilt [50] and Zhong *et al.* [51] report phonon frequencies for the FE-phonon mode [Γ_{15} (TO1)] that differ by over 80 cm^{-1}, although their applied lattice constants and exchange-correlation functionals are identical. Moreover, Sai and Vanderbilt [50] found the mode to be hard, whereas Zhong *et al.* [51] predicted it to be soft, indicating a ferroelectric instability. Additionally Tinte *et al.*,[40] Sai and Vanderbilt,[50] and Ghosez *et al.*[56] also used the experimental lattice constant for their calculations, which induces an external, fictitious negative pressure on the systems unit cell.

Such a situation is certainly discomforting and it reflects the difficulties in the construction of suitable pseudopotentials for Ti, and the rather slow convergence of the low-frequency branch with respect to the number of k points. The present calculations were performed using a full potential method, and treating the entire Ti 3s, 3p, and 3d shell as valence in order to avoid any errors related to the frozen core approximation applied in our PAW calculations. Furthermore, it is nowadays certainly possible to fully converge the results with respect to the k-point set for local and gradient-corrected functionals; however, for the hybrid functionals computational costs increase like the square of the number of k points, and therefore certain compromises were required. To remain concise, the same set of k points was used for all

TABLE IV. Comparison of calculated and experimental direct $\Gamma-\Gamma$ (and indirect $R-\Gamma$ band gap) in electronvolts for cubic and tetragonal distorted $SrTiO_3$ and $BaTiO_3$.

	LDA		PBE		PBEsol		HSE		B3LYP		B3PW		WC		B1-WC		Exp.	
								Cubic										
$SrTiO_3$																		
Present	2.15	(1.81)	2.18	(1.80)	2.18	(1.82)	3.47	(3.07)									3.75[a]	(3.25[a])
Ref. 38	2.36	(2.04)	2.35	(1.99)					3.96	(3.63)	3.89	(3.57)						
Ref. 4															3.91	(3.57)		
$BaTiO_3$																		
Present	1.84	(1.73)	1.87	(1.70)	1.91	(1.77)	3.07	(2.92)										(3.2[b])
Ref. 4	2.2	(2.1)	2.2	(2.1)					3.8	(3.7)			2.2	(2.1)	3.45	(3.39)		
								Tetragonal										
$SrTiO_3$																		
Present	2.21	(1.97)	2.12	(1.79)	2.21	(1.93)	3.48	(3.11)										
Ref. 5											4.03	(3.72)						
$BaTiO_3$																		
Present	2.09	(1.84)	2.31	(1.76)	2.16	(1.76)	3.55	(3.02)										(3.4[b])
Ref. 4		(2.10)								(3.80)					3.73	(3.44)		

[a]Reference 47.
[b]Reference 48.

calculations ($6\times6\times6$), and hence the error bar for the low-frequency imaginary branch might approach 10 cm^{-1}.

Before discussing the behavior of the low-frequency mode in more detail, we first want to elaborate briefly on the other modes. It is obvious that LDA performs quite well in predicting the vibrational frequencies. The Γ_{15} (TO2) and the Γ_{15} (TO3) modes match almost exactly the experimental data for both STO, as well as BTO, despite—or rather because—the calculations were done at the LDA volume, which is significantly too small. The PBE functional generally yields much too soft modes at the theoretical PBE volume. We note that most phonon modes are fairly independent of the applied functional, and the difference between LDA and GGA is mainly related to the different volume at which the calculations were performed. As a result of the intermediate volume, the PBEsol functional yields values pretty much in between

TABLE V. Zone-center phonon frequencies for the cubic structure of $SrTiO_3$. In the second column we give the used lattice constant (in Å) for the calculations and the temperature (in K) for the experimental data [Tinte *et al.* (Ref. 40) and Ghosez *et al.* (Ref. 49) used the experimental lattice constant in their calculations, Sai and Vanderbilt (Ref. 50) used it also for comparison to the theoretical lattice constant].

Work	(Å)		Γ_{15} (TO1) (cm^{-1})	Γ_{15} (TO2) (cm^{-1})	Γ_{25} (cm^{-1})	Γ_{15} (TO3) (cm^{-1})
Present work	3.863	LDA	80	177	226	563
Present work	3.943	PBE	115*i*	147	234	512
Present work	3.898	PBEsol	29*i*	160	229	536
Present work	3.904	HSE	74*i*	162	250	533
Ref. 49	3.904	LDA	87*i*	149	223	519
Ref. 50	3.865	LDA	42	168		549
	3.897	LDA	94*i*	151		521
Ref. 51	3.865	LDA	41*i*	165		546
Ref. 40	3.894	LDA	57*i*	157		532
	3.894	GGA	64	166		551
Ref. 52	296 °K	Exp	91.1			
Ref. 52	90 °K	Exp	42.3	170	265	
Ref. 21	120 °K	Exp	52.5			
Ref. 53	300 °K	Exp	87.7	178		544
Ref. 54	297 °K	Exp	91.7	169 ± 3	265 ± 5	547 ± 3
Ref. 55	295 °K	Exp	88 ± 1	175 ± 2	266 ± 3	545 ± 1

TABLE VI. Zone-center phonon frequencies for the cubic structure of $BaTiO_3$. In the second column we give the used lattice constant (in Å) for the calculations and the temperature (in K) for the experimental data.

Work	(Å)		Γ_{15} (TO1) (cm^{-1})	Γ_{15} (TO2) (cm^{-1})	Γ_{25} (cm^{-1})	Γ_{15} (TO3) (cm^{-1})
Present work	3.953	LDA	139*i*	186	291	479
Present work	4.035	PBE	239*i*	169	286	453
Present work	3.986	PBEsol	188*i*	178	287	465
Present work	3.995	HSE	241*i*	185	310	480
Ref. 56	3.94	LDA	113*i*	184	288	481
Ref. 40	4.03	PBE	203*i*	168		463
Ref. 4	3.990	WC	128*i*	186	282	469
Ref. 4	3.971	B1-WC	145*i*	195	299	482
Ref. 57	395 °K	Exp	soft	182	308	482

the LDA and PBE. If the results were entirely independent of the functional, one would expect similar values for the HSE functional. But this is not generally the case. On the contrary, inclusion of exact exchange stiffens the bonds somewhat and increases the phonon frequencies by typically 5% compared to a local or gradient-corrected functional. This behavior is well known for molecules,[58] and is also observed for extended bulk systems.[59] Here we also observe that the HSE functional yields consistently larger phonon frequencies than the PBEsol functional, although the equilibrium volume is slightly larger for HSE than for PBEsol. For BTO, the agreement is exceptionally good, whereas some discrepancies remain for the STO case. But even for STO the HSE functional yields overall the best agreement with experiment. We emphasize that the frequency of the fairly volume-independent Γ_{25} mode is only accurately described by the HSE functional, whereas all nonhybrid functionals underestimate its frequency.

We now return to the low-frequency "soft" mode. Even our own data show a large scatter among the four applied functionals, and to clarify whether these differences are related to different equilibrium volumes or to the applied exchange-correlation functional, we investigated the volume dependence of the phonon modes of STO and BTO for all applied functionals. The AFD mode, corresponding to the zone boundary phonon at the *R* point, was included in this investigation by doubling the unit cell, as already described in Sec. III A.

The results confirm our previous discussion. Most of the phonon modes are quite insensitive to the applied functional, although as already discussed the hybrid HSE functional shows a tendency to stiffen the modes, in particular the Γ_{25} mode. Even the imaginary frequency of the AFD mode only slightly depends on the functional, but we recall that the final displacement pattern, which also depends on quadratic terms, showed a strong dependence on the functional (see Table II). The frequency of the ferroelectric mode, however, clearly changes from one functional to the other. This applies to both STO, as well as BTO. We see that the mode becomes soft upon increasing the volume. For STO the transition occurs very close to the experimental (and PBEsol and HSE) volume. A very simple model that is capable to describe the observed behavior is now discussed.

Whether (S,B)TO is unstable against a ferroelectric instability seems to be determined by the space available to the Ti atom in the O-octahedron cage and by the preferred Ti-O distance. The space available to the Ti atom is proportional to half of the lattice constant. To determine the preferred Ti–O bond length, we optimized the TiO_2 rutile structure for each of the considered potentials and determined the respective theoretical Ti–O bond length in this structure. The relevant values are given in the first line of Table VII.

Indeed, the table suggests that at the theoretical equilibrium volume, the FE mode of STO is stable in the LDA ($a_{STO}/2=1.931<1.932$), strongly unstable for PBE ($a_{STO}/2=1.972>1.962$), and slightly unstable for PBEsol

TABLE VII. Comparison of equilibrium M(=Ti,Sr,Ba)–O bond lengths (in Å). As reference for the stable metal-oxide bulk structures, the rutile (TiO_2) and the NaCl structure (SrO and BaO) were used. For STO and BTO the cubic structure was used. The numbers in parentheses give the percental deviations of the equilibrium distances from experiment.

Bond		LDA	PBE	PBEsol	HSE	Exp.
Ti–O	TiO_2	1.932(−0.8%)	1.962(+0.7%)	1.945(−0.2%)	1.944(−0.3%)	1.949
	$SrTiO_3$	1.931(−1.0%)	1.972(+1.1%)	1.949(−0.1%)	1.952(+0.1%)	1.950
	$BaTiO_3$	1.976(−1.2%)	2.018(+0.9%)	1.993(−0.3%)	1.997(−0.1%)	2.000
Sr–O	SrO	2.538(−1.6%)	2.602(+0.9%)	2.567(−0.5%)	2.583(+0.1%)	2.580
	$SrTiO_3$	2.731(−1.0%)	2.788(+1.1%)	2.756(−0.1%)	2.760(+0.1%)	2.758
Ba–O	BaO	2.739(−1.1%)	2.807(+1.4%)	2.767(−0.1%)	2.787(+0.6%)	2.770
	$BaTiO_3$	2.795(−1.2%)	2.853(+0.9%)	2.819(−0.3%)	2.825(−0.1%)	2.828

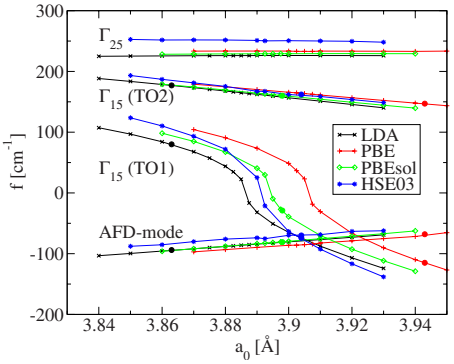

FIG. 3. (Color online) Volume dependence of the AFD and FE-phonon mode of STO. Imaginary frequencies are represented by negative numbers. Phonon frequencies at the equilibrium volume are highlighted by filled circles.

and HSE. This agrees with the predictions in Fig. 3. Furthermore, the lattice constants at which the instability is theoretically predicted to occur ($a_{STO}/2=1.939$, 1.947, 1.948, and 1.953 Å for LDA, HSE, PBEsol, and PBE, respectively) possess the same order as the preferred theoretical Ti–O bond lengths.

Comparison with experiment suggests that both HSE and PBEsol predict the $SrTiO_3$ volume and the preferred Ti–O bond length in TiO_2 reasonably well, the PBEsol functional more so than HSE. LDA more strongly underestimates the $SrTiO_3$ volume, and therefore predicts $SrTiO_3$ to be stable against a FE distortion of the lattice at the theoretical volume, whereas PBE predicts a much too large volume for $SrTiO_3$ and therefore overestimates the instability at the theoretical volume.

For BTO the transition from hard to soft is observed far below the equilibrium volume, at lattice constants only slightly larger than those of STO, as can be seen from Fig. 4. The $a_{BTO}/2$ distances at the transition are 1.962, 1.963, 1.964, and 1.966 Å for HSE, LDA, PBEsol, and PBE—all well below the respective equilibrium Ti-O distances in BTO but only slightly larger than Ti-O in TiO_2. Thus BTO is without question, and for all applied functionals, a ferroelectric material, whereas STO is just on the fringe of a ferroelectric instability, making it difficult to place a firm number on the frequency of the Γ_{15}(TO1) mode. Fortunately, HSE and PBEsol, both functionals that predict reasonable equilibrium volumes and Ti–O bond lengths, show that $SrTiO_3$ is indeed unstable against a ferroelectric distortion, in agreement with the conclusion one must draw from the available experimental data.

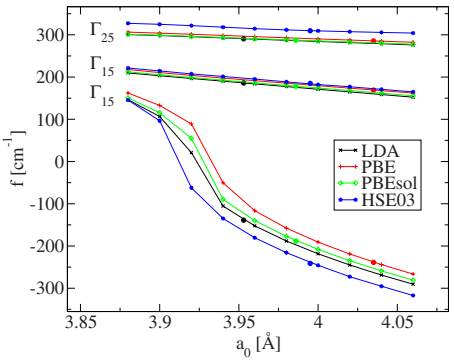

FIG. 4. (Color online) FE-phonon mode for different lattice constants for cubic $BaTiO_3$. Imaginary frequencies are presented by negative numbers. Phonon frequencies at the equilibrium volume are denoted by filled circles.

IV. SUMMARY AND CONCLUSION

In the present study, we have shown that the use of the novel PBEsol and HSE functionals gives a significant improvement of the description of the ABO_3 perovskites $SrTiO_3$ and $BaTiO_3$ in their cubic and tetragonal phases. Whereas the equilibrium geometries are sufficiently well captured by PBEsol (being a "classical" GGA potential with just the scaling coefficients adapted to improve the structural properties of solids and surfaces), it is inevitable to admix exact nonlocal Fock exchange to the standard density functional, as done in HSE, in order to obtain accurate electronic structure results. Only the latter approach gives satisfactory agreement of the calculated band gaps with experiment.

Furthermore, our results show that the ferroelectric instability strongly depends on the volume and to a lesser extent on the applied functional. Specifically, a transition from a hard ferroelectric mode at small volumes to a soft mode at larger volumes is predicted, with the transition occurring roughly at the equilibrium volume of $SrTiO_3$. This makes it so particularly hard to predict whether $SrTiO_3$ is unstable toward a ferroelectric distortion or not. Maybe the most crucial result of our study is that the lattice constant at which the transition is predicted to occur is roughly twice the theoretical equilibrium TiO bond length in TiO_2. This relation is clearly observed for $SrTiO_3$, but it also approximately applies to $BaTiO_3$. Since the Ti–O bond length in TiO_2 varies greatly between the functionals, quite different transition points are observed in $SrTiO_3$. Because LDA generally predicts too short bonds, and GGA generally predicts too large bonds, the best strategy seems to judge the stability of the mode by calculating its frequency at the theoretical equilibrium volume. Such a strategy should take care of the fact that the LDA and GGA "worlds" are too small and large, respectively, but unfortunately the strategy fails. The local density approximation more severely underestimates the Sr–O bond length than the Ti–O bond length. Therefore the $SrTiO_3$ volume, which is a compromise between Ti–O and Sr–O bonds, is much too small and the Ti atoms are locally confined without the ability to undergo an off center movement. The usual gradient-corrected functional (PBE) shows the opposite trend, with a more severe overestimation of the Sr–O bond length than the Ti–O bond length. In this case, the ferroelectric instability is most likely overestimated at the theoretical $SrTiO_3$ equilibrium volume. The HSE functional predicts 1% smaller lattice constants than PBE, but the relative bond length errors are very similar to PBE. For this particular problem, the PBEsol functional seems to offer the best compromise with accurate predictions for all bonds (Sr–O, Ti–O, and Ba–O).

The semilocal exchange functional suggested by Wu and Cohen (WC) (Ref. 6) works very similar as PBEsol in most

respects. This is related to the fact that the PBEsol functional modifies the semilocal exchange in very much the same manner as Wu and Cohen suggested for their WC functional. The hybrid B1–WC functional,[4] which combines the WC functional with 16% nonlocal exchange, yields slightly too small lattice constants, since the inclusion of nonlocal exchange always shrinks the lattice constants compared to the corresponding semilocal functional [typical errors for $BaTiO_3$ and $SrTiO_3$ are −1% (see Ref. 4)]. On the other hand, the HSE functional tends to overestimate the volumes slightly, a behavior that it carries over from its parent PBE functional (errors for $BaTiO_3$ and $SrTiO_3$ are 1%). Whether B1-WC or HSE are ultimately better suited for a specific problem might be largely system dependent, but we note that for $BaTiO_3$ and $PbTiO_3$, B1-WC predicts exceptionally good ferroelectric displacements and polarizations (at slightly too small equilibrium volumes).

Our important conclusion is that a design goal of functionals is the proper prediction of the *bond length balance* in very diverse materials. Although obvious in hindsight, this statement is hardly ever borne out as clearly as in the present study. It is noted that this observation applies to many other problems, for instance, strain and stress relief at interfaces.

Since the PBEsol and WC functionals work so exceptionally well, the question arises, whether there is any need for hybrid functionals. After all, they are at least one order of magnitude more expensive than semilocal functionals, and the PBEsol and WC functionals just work exceedingly well for $BaTiO_3$ and $SrTiO_3$. So, why bother with a huge increase in computational costs? In fact, apart from the band gaps, which are arguably not ground-state properties, there are a few other properties that are predicted clearly better by the hybrid functionals. For $SrTiO_3$ the ground-state structure of the distorted antiferroelectric phase is in better agreement with experiment for the hybrid functional HSE, whereas all local functionals predict a somewhat too strong distortion. Second, the phonon modes are much more accurate using the hybrid functionals. In fact, the only other functional that allows for a reasonable prediction of the phonon frequencies is the LDA, if the frequencies are evaluated at the theoretically predicted equilibrium volume. LDA predicts so good frequencies because of a sizeable error compensation: LDA frequencies at the experimental volume are too soft, but the too small volume and the strong increase in the phonons with volume compensates for this. GGA drastically underestimates the phonon frequencies as a result of a too large equilibrium volume, and as a result of a general underestimation of phonon frequencies using semilocal functionals. The hybrid functionals (HSE and B1-WC) work exceptionally well, and they are in fact the only functionals that allow to make accurate predictions for the Γ_{25} mode.

The verdict on which functional to prefer for ferroelectric materials is certainly still open and requires further theoretical investigations. At this point it is only clear that theory is moving in the right direction. Both, the revised PBEsol functional and the WC functional, as well as the hybrid HSE and B1-WC functionals, are capable to make reliable predictions for $SrTiO_3$ and $BaTiO_3$, avoiding many problems inherent to the PBE and LDA functionals.

ACKNOWLEDGMENTS

We want to thank Martijn Marsman for helpful discussions and Joachim Paier for the implementation of the PBEsol functional in VASP. R. W. gratefully acknowledges financial support by the Austrian Science Foundation (FWF), Project No. W401-N13.

[1] P. Hohenberg and W. Kohn, Phys. Rev. **136**, B864 (1964).
[2] W. Kohn and L. J. Sham, Phys. Rev. **140**, A1133 (1965).
[3] J. P. Perdew, K. Burke, and M. Ernzerhof, Phys. Rev. Lett. **77**, 3865 (1996).
[4] D. I. Bilc, R. Orlando, R. Shaltaf, G.-M. Rignanese, J. Íñiguez, and Ph. Ghosez, Phys. Rev. B **77**, 165107 (2008).
[5] E. Heifets, E. Kotomin, and V. A. Trepakov, J. Phys.: Condens. Matter **18**, 4845 (2006).
[6] Z. Wu and R. E. Cohen, Phys. Rev. B **73**, 235116 (2006).
[7] J. P. Perdew, A. Ruzsinsky, G. I. Csonka, O. A. Vydrov, G. E. Scuseria, L. A. Constantin, X. Zhou, and K. Burke, Phys. Rev. Lett. **100**, 136406 (2008).
[8] R. Armiento and A. E. Mattsson, Phys. Rev. B **72**, 085108 (2005).
[9] A. E. Mattsson, R. Armiento, J. Paier, G. Kresse, J. M. Wills, and T. R. Mattson, J. Chem. Phys. **128**, 084714 (2008).
[10] M. Shishkin, M. Marsman, and G. Kresse, Phys. Rev. Lett. **99**, 246403 (2007).
[11] P. J. Stephens, F. J. Devlin, C. F. Chabalowski, and M. J. Frisch, J. Phys. Chem. **98**, 11623 (1994).
[12] C. Adamo and V. Barone, J. Chem. Phys. **110**, 6158 (1999).
[13] M. Ernzerhof and G. E. Scuseria, J. Chem. Phys. **110**, 5029 (1999).
[14] A. V. Krukau, O. A. Vydrov, A. F. Izmaylov, and G. E. Scuseria, J. Chem. Phys. **125**, 224106 (2006).
[15] J. Muscat, A. Wander, and N. M. Harrison, Chem. Phys. Lett. **342**, 397 (2001).
[16] J. Heyd, J. E. Peralta, G. E. Scuseria, and R. L. Martin, J. Chem. Phys. **123**, 174101 (2005).
[17] J. Paier, M. Marsman, K. Hummer, G. Kresse, I. C. Gerber, and J. G. Ángyán, J. Chem. Phys. **124**, 154709 (2006); **125**, 249901(E) (2006).
[18] J. Paier, M. Marsman, and G. Kresse, J. Chem. Phys. **127**, 024103 (2007).
[19] M. Liu, T. R. Finlayson, and T. F. Smith, Phys. Rev. B **55**, 3480 (1997).
[20] L. Cao, E. Sozontov, and J. Zegenhagen, Phys. Status Solidi A **181**, 387 (2000).
[21] G. Shirane and Y. Yamada, Phys. Rev. **177**, 858 (1969).
[22] G. Shirane, H. Danner, and P. Pepinsky, Phys. Rev. **105**, 856 (1957).
[23] K. A. Müller and H. Burkard, Phys. Rev. B **19**, 3593 (1979).
[24] G. Rupprecht and R. O. Bell, Phys. Rev. **125**, 1915 (1962).
[25] R. Viana, P. Lunkenheimer, J. Hemberger, R. Böhmer, and A.

Loidl, Phys. Rev. B **50**, 601 (1994).
[26] H. Uwe and T. Sakudo, Phys. Rev. B **13**, 271 (1976).
[27] M. Itoh, R. Wang, Y. Inaguma, T. Yamaguchi, Y.-J. Shan, and T. Nakamura, Phys. Rev. Lett. **82**, 3540 (1999).
[28] W. Jauch and A. Palmer, Phys. Rev. B **60**, 2961 (1999).
[29] W. Zhong and D. Vanderbilt, Phys. Rev. B **53**, 5047 (1996).
[30] G. H. Kwei, A. C. Lawson, and S. J. L. Billinge, J. Phys. Chem. **97**, 2368 (1993).
[31] G. Kresse and J. Furthmüller, Comput. Mater. Sci. **6**, 15 (1996).
[32] G. Kresse and J. Furthmüller, Phys. Rev. B **54**, 11169 (1996).
[33] H. J. Monkhorst and J. D. Pack, Phys. Rev. B **13**, 5188 (1976).
[34] J. P. Perdew, M. Ernzerhof, and K. Burke, J. Chem. Phys. **105**, 9982 (1996).
[35] J. Heyd, G. E. Scuseria, and M. Ernzerhof, J. Chem. Phys. **118**, 8207 (2003).
[36] *Ferroelectrics and Related Substances*, edited by K. H. Hellwege and A. M. Hellwege, Landolt-Börnstein, New Series, Group III, Vol. 3 (Springer-Verlag, Berlin, 1969).
[37] E. Heifets, R. I. Eglitis, E. A. Kotomin, J. Maier, and G. Borstel, Phys. Rev. B **64**, 235417 (2001).
[38] S. Piskunov, E. Heifets, R. I. Eglitis, and G. Borstel, Comput. Mater. Sci. **29**, 165 (2004).
[39] E. Mete, R. Shaltaf, and Ş. Ellialtıoğlu, Phys. Rev. B **68**, 035119 (2003).
[40] S. Tinte, M. G. Stachiotti, C. O. Rodriguez, D. L. Novikov, and N. E. Christensen, Phys. Rev. B **58**, 11959 (1998).
[41] B. Alefeld, Z. Phys. **222**, 155 (1969).
[42] A. Heidemann and H. Wettengel, Z. Phys. **258**, 429 (1973).
[43] H. Unoki and T. Sakudo, J. Phys. Soc. Jpn. **23**, 546 (1967).
[44] H. H. Wieder, Phys. Rev. **99**, 1161 (1955).
[45] R. D. King-Smith and D. Vanderbilt, Phys. Rev. B **47**, 1651 (1993); D. Vanderbilt and R. D. King-Smith, *ibid.* **48**, 4442 (1993).
[46] R. Resta, Rev. Mod. Phys. **66**, 899 (1994).
[47] K. van Benthem, C. Elsässer, and R. H. French, J. Appl. Phys. **90**, 6156 (2001).
[48] S. H. Wemple, Phys. Rev. B **2**, 2679 (1970).
[49] P. Ghosez, D. Desquesnes, X. Gonze, and K. M. Rabe, *Fundamental Physics of Ferroelectrics 2000: Aspen Center for Physics Winter Workshop*, AIP Conf. Proc. No. 535 (AIP, New York, 2000), p. 102.
[50] N. Sai and D. Vanderbilt, Phys. Rev. B **62**, 13942 (2000).
[51] W. Zhong, R. D. King-Smith, and D. Vanderbilt, Phys. Rev. Lett. **72**, 3618 (1994).
[52] R. A. Cowley, Phys. Rev. **134**, A981 (1964).
[53] W. G. Spitzer, R. C. Miller, D. A. Kleinman, and L. E. Howarth, Phys. Rev. **126**, 1710 (1962).
[54] W. G. Stirling, J. Phys. C **5**, 2711 (1972).
[55] H. Vogt and G. Neumann, Phys. Status Solidi B **92**, 57 (1979).
[56] P. Ghosez, X. Gonze, and J.-P. Michenaud, Europhys. Lett. **33**, 713 (1996).
[57] Y. Luspin, J. L. Servoin, and F. Gervais, J. Phys. C **13**, 3761 (1980).
[58] A. P. Scott and L. Radom, J. Phys. Chem. **100**, 16502 (1996).
[59] K. Hummer and G. Kresse (unpublished).